SUPERCONDUCTIVITY

Antiferroic electronic structure in the nonmagnetic superconducting state of the iron-based superconductors

Takahiro Shimojima,[1,2*†] Walid Malaeb,[2,3] Asuka Nakamura,[1] Takeshi Kondo,[2] Kunihiro Kihou,[4] Chul-Ho Lee,[4] Akira Iyo,[4] Hiroshi Eisaki,[4] Shigeyuki Ishida,[4] Masamichi Nakajima,[5] Shin-ichi Uchida,[6] Kenya Ohgushi,[7] Kyoko Ishizaka,[1] Shik Shin[2*]

A major problem in the field of high-transition temperature (T_c) superconductivity is the identification of the electronic instabilities near superconductivity. It is known that the iron-based superconductors exhibit antiferromagnetic order, which competes with the superconductivity. However, in the nonmagnetic state, there are many aspects of the electronic instabilities that remain unclarified, as represented by the orbital instability and several in-plane anisotropic physical properties. We report a new aspect of the electronic state of the optimally doped iron-based superconductors by using high–energy resolution angle-resolved photoemission spectroscopy. We find spectral evidence for the folded electronic structure suggestive of an antiferroic electronic instability, coexisting with the superconductivity in the nonmagnetic state of $Ba_{1-x}K_xFe_2As_2$. We further establish a phase diagram showing that the antiferroic electronic structure persists in a large portion of the nonmagnetic phase covering the superconducting dome. These results motivate consideration of a key unknown electronic instability, which is necessary for the achievement of high-T_c superconductivity in the iron-based superconductors.

INTRODUCTION

One of the most intriguing properties of the iron-based superconductors (IBSCs) (*1*) is the high-transition temperature (T_c) superconductivity in balance with the multiple instabilities in lattice, spin, and orbital degrees of freedom. To understand the origin of high T_c, it is important to elucidate the nature of these electronic instabilities and their relations to the superconductivity. As represented by the phase diagram of $Ba_{1-x}K_xFe_2As_2$ (BaK122) in Fig. 1A (*2*), most of the parent IBSCs exhibit the stripe-type antiferromagnetic (AFM) order at T_N (*3*, *4*). A tetragonal-to-orthorhombic structural transition occurs just at or slightly above T_N (T_s). It accompanies a spontaneous difference in the occupation of Fe $3d_{xz}$ and $3d_{yz}$ orbitals being much larger than that expected from the orthorhombicity (*5*–*7*), namely, the ferro-orbital order (*8*–*10*). The structural transition has been suggested to be a nematic order (*11*, *12*) driven by fluctuating antiferromagnetism (*13*–*15*) and/or orbital ordering (*16*–*18*).

Whereas these orders are suppressed by carrier doping, many indications of electronic instabilities have been found in the normal state of IBSCs. Twofold symmetric physical properties were observed above T_N/T_s in the underdoped regime, as represented by in-plane electronic resistivity (*19*) for $Ba(Fe_{1-x}Co_x)_2As_2$ (FeCo122) and magnetic torque measurements (*20*) for $BaFe_2(As_{1-x}P_x)_2$. AFM fluctuations and nematic fluctuations were reported to extend over the whole superconducting (SC) dome of BaK122 by the neutron magnetic resonance (NMR) (*21*) and shear modulus measurements (*22*), respectively. In addition, the ferro-orbital order/fluctuation detected by x-ray linear dichroism measurement was found to persist in the optimally doped (OP) regime of FeCo122 (*23*). These observations indicate that superconductivity in IBSCs, especially the 122 system, is subject to the influence of multiple electronic instabilities. However, the normal-state electronic structure in the OP regime has been reported to exhibit the tetragonal symmetry without any sign of electronic instability. Here, we report the spectral evidence for the antiferroic electronic structure in the normal state of the OP BaK122. Previous angle-resolved photoemission spectroscopy (ARPES) measurements on BaK122 mainly focused on the SC gap distribution in the multiorbital Fermi surfaces (FSs) (*24*–*32*). Here, we systematically investigate fine electronic structures at both the Brillouin zone (BZ) center (Γ) and corner (*X*) of the BaK122 system by using high–energy resolution ARPES. Across the SC transition of the OP sample, we observe a drastic change in the electron band at *X* point, together with the evolution of an unusual intensity distribution around Γ point. Striking resemblances in *E*, *k*, and *T* dependences between these two electronic features suggest that the latter is a replica of the former. We establish the *x*-*T* phase diagram ($0.18 \leq x \leq 0.69$ and $5\ K \leq T \leq 200\ K$) showing that this antiferroic electronic instability persists in a large portion of the nonmagnetic phase covering the SC dome.

RESULTS

Electronic structure around *X* point

Figure 1B shows the FSs of OP BaK122 obtained in the normal state ($T = 40$ K). The schematic in Fig. 1C shows two hole pockets centered at Γ point and a small electron pocket with flower-like hole pockets around *X* point (section S1), as similarly reported in a previous ARPES study (*26*). Here, we start with a description of the electronic structure around *X* point for the OP $x = 0.41$. As indicated in the *E*-*k* images along the momentum cut 1 (Fig. 1C) divided by the Fermi-Dirac function (Fig. 1, D and F), the electron band at *X* point shows a drastic change in its shape across T_c (36 K). Above T_c, the bottom of the parabolic electron band locates at a binding energy of ~8 meV. The shallow electron band is consistent with the rigid band picture, which predicts the band shift of ~40 meV toward lower binding energy with respect to

[1]Quantum-Phase Electronics Center and Department of Applied Physics, University of Tokyo, Bunkyo, Tokyo 113-8656, Japan. [2]Institute for Solid State Physics, University of Tokyo, Kashiwa, Chiba 277-8581, Japan. [3]Department of Physics, Faculty of Science, Beirut Arab University, Beirut 11-5020, Lebanon. [4]National Institute of Advanced Industrial Science and Technology, Tsukuba, Ibaraki 305-8568, Japan. [5]Department of Physics, Osaka University, 1-1 Machikaneyama-cho, Toyonaka, Osaka 560-0043, Japan. [6]Department of Physics, University of Tokyo, Bunkyo, Tokyo 113-0033, Japan. [7]Department of Physics, Graduate School of Science, Tohoku University, 6-3, Aramaki Aza-Aoba, Aoba-ku, Sendai, Miyagi 980-8578, Japan.
*Corresponding author. Email: takahiro.shimojima@riken.jp (T.S.); shin@issp.u-tokyo.ac.jp (S.S.)
†Present address: RIKEN Center for Emergent Matter Science, Wako 351-0198, Japan.

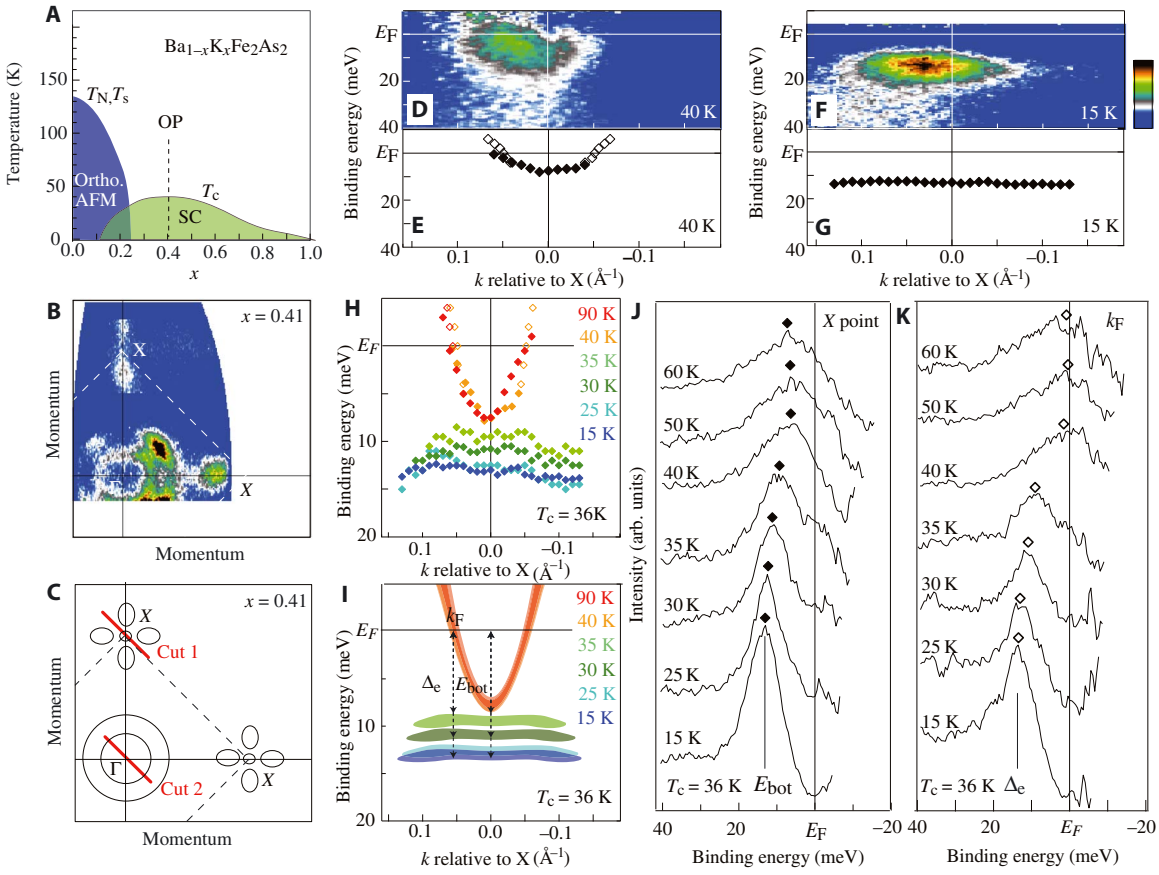

Fig. 1. Temperature-dependent ARPES around *X* point for $Ba_{0.59}K_{0.41}Fe_2As_2$. (**A**) Phase diagram of BaK122 (*2*). T_N and T_s are nearly equivalent in this system. (**B**) FSs of OP BaK122 obtained at 40 K with the photons of $h\nu$ = 21.2 eV. (**C**) Schematic of (B). (**D**) *E*-*k* image divided by the Fermi-Dirac function taken at 40 K along cut 1 in (C). (**E**) Peak positions of the EDCs (filled diamonds) and momentum distribution curves (MDCs) (open diamonds) in (D). (**F** and **G**) The same as (D) and (E), but obtained at 15 K. (**H**) *T* dependence of the peak plots around *X* point from 15 to 90 K. (**I**) Schematic of (H). Δ_e and E_{bot} represent the SC gap magnitude of the electron band and energy level of the band bottom, respectively. (**J** and **K**) *T* dependence of the EDCs divided by the Fermi-Dirac functions at *X* point and k_F of the electron band (k = 0.06 Å^{-1}), respectively.

the parent Ba122 (*33*). As indicated by the peak positions of the energy distribution curves (EDCs) in Fig. 1 (E, G, and H) (section S2), the electron band becomes anomalously flat in the SC state. This result is understood by considering the SC gap (Δ_e) formation at the Fermi momentum (k_F) with an energy scale comparable to that of the electron band bottom (E_{bot}), as depicted in Fig. 1I. The condition of $\Delta_e \approx E_{bot}$ can be regarded as a SC state in the Bardeen-Cooper-Schrieffer (BCS)–Bose-Einstein condensation crossover regime where the Fermi energy and SC gap magnitude are comparable, as has been discussed in the FeSe family (*34*–*36*). In the Ba122 family, this circumstance is realized only in the hole-doped system because E_{bot} for the parent Ba122 (~50 meV) is much larger than Δ_e of any ion-substituted Ba122 (*33*).

In addition to the drastic change of the band shape, we observed the shift of E_{bot} to the higher binding energy below T_c. For the quantitative analysis, we show the EDCs at *X* point in Fig. 1J. The peaks of the EDCs, representing the electrons at the band bottom, are remarkably enhanced below T_c and simultaneously shift toward higher binding energy by ~6 meV. On the other hand, the EDCs at the k_F of the electron band exhibit finite SC gap formation below T_c (Fig. 1K). The characteristic shift in the band bottom seems to occur when Δ_e becomes comparable to E_{bot} with decreasing *T* (Fig. 1I), which implies that the superconductivity modifies the band structure.

Electronic structure around Γ point

Next, we performed detailed *T*-dependent ARPES at Γ point by using laser-ARPES (*37*, *38*) along the momentum cut 2 in Fig. 1C. In the normal state, we observed an inner hole band around Γ point crossing the E_F in the *E*-*k* image (Fig. 2, A and E). To clearly see the *T* dependence, we show the EDCs at the k_F of the inner hole band in Fig. 2I (along the dashed lines in Fig. 2, A to D) and those divided by the Fermi-Dirac function and further normalized by that at 60 K in Fig. 2J. As *T* decreased, we observed the evolution of a peak and a gap structure near E_F below T_c. The counterparts of the peak in the unoccupied state (Fig. 2, I and J) and its *T* dependence characterized by the BCS curve (Fig. 2K) suggest that these spectral features represent the SC gap formation in the inner hole band ($\Delta_h \leq$ 5 meV). We further observed a flat intensity distribution appearing at E_{flat} = ~10 meV around Γ point (Fig. 2, A to D), as similarly observed in previous ARPES studies (*24*–*30*, *32*). We note that the flat feature cannot be explained by the first-principles band calculations assuming the paramagnetic state and tetragonal lattice (*39*). Peak plots obtained from EDCs and MDCs in Fig. 2 (E to H) exhibit the evolution of the SC gap and flat feature across T_c (section S3). In addition to the SC peaks, the EDCs in Fig. 2I exhibit a sharp peak at E_{flat}. Note that the flat feature becomes apparent below T_c and exhibits an energy shift toward higher binding

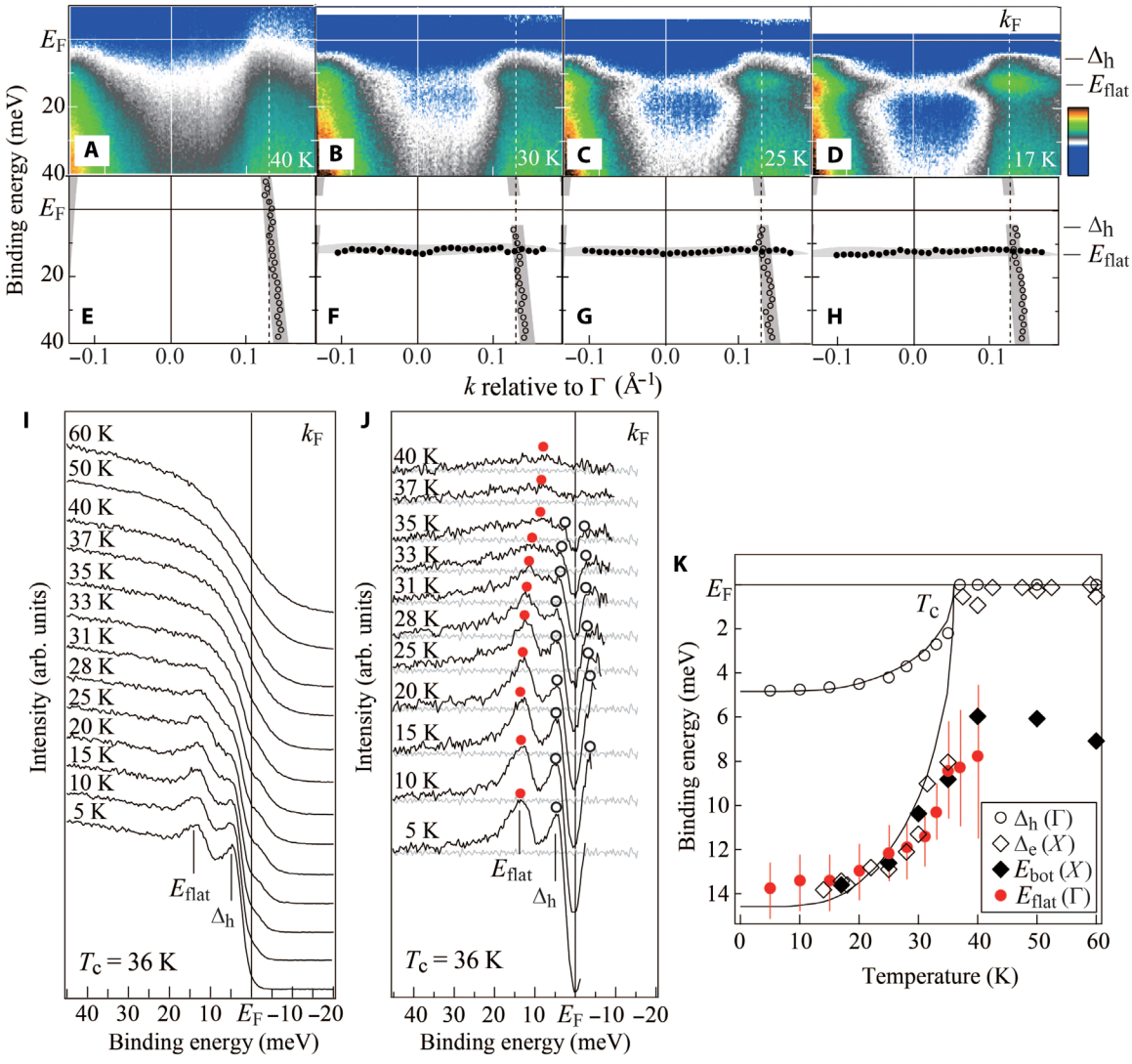

Fig. 2. Temperature-dependent ARPES around Γ point for $Ba_{0.59}K_{0.41}Fe_2As_2$. (**A** to **D**) T dependence of E-k images divided by the Fermi-Dirac functions obtained by laser-ARPES ($h\nu$ = 6.994 eV) along cut 2 in Fig. 1C. (**E** to **H**) Peak plots obtained from EDCs (filled circles) and MDCs (open circles) in (A) to (D). Gray curves are guides to the eye. Δ_h and E_{flat} represent the SC gap magnitude of the inner hole band and the energy level of the flat intensity distribution at k_F, respectively. (**I**) T dependence of the EDCs at k_F of inner hole band. (**J**) The EDCs in (I) divided by the Fermi-Dirac functions and further normalized by that at 60 K. The data set shown in (I) and (J) was taken from Shimojima *et al.* (*28*). (**K**) T dependences in the energy levels of Δ_h, Δ_e, E_{bot}, and E_{flat}. Black solid curves represent the BCS curves for hole and electron bands.

energy with decreasing T, as shown by the red markers in Fig. 2J (section S4). Because the flat feature responds to the onset of the superconductivity, it should reflect the bulk electronic properties of OP BaK122.

Temperature dependences of the electronic features in Γ and *X* points

Here, we compare the energy levels of Δ_h, Δ_e, E_{bot}, and E_{flat} in Fig. 2K. In the SC state, both Δ_h and Δ_e follow the BCS-like T dependence, as indicated by the black solid curves. E_{bot} exhibits the energy shift comparable to that of Δ_e, resulting in the flat electron band at X point below T_c. We further found that the energy shift in E_{flat} is also in good agreement with those of Δ_e and E_{bot}, suggesting that the unidentifiable flat feature around Γ point has a close relation to the electronic structure around X point. Because the flat feature around Γ point shows a striking resemblance to the flat electron band at X point in its k, E, and T dependences, we here assign the former as a replica of the latter (section S5). This replica indicates the antiferroic band folding between Γ and X points, characterized by the same wave vector as the AFM order in the parent Ba122 [denoted as (π,π) folding in Fig. 3A] (*3*).

We summarize our observations in the simplified schematic images. According to the E-k images in Figs. 1D and 2A, the electronic structure in the normal state can be depicted by a hole band and an electron band in Fig. 3B. Far below T_c, the SC gaps were observed in both hole and electron bands with Δ_h = 5 meV and Δ_e = 14 meV, respectively (Fig. 3C). In the presence of the (π,π) folding, the electron band at X point will be overlapped with the hole band at Γ point (Fig. 3D), which should correspond to the appearance of the flat feature around Γ point in the present ARPES data. This picture is consistent with two main observations in the present study for OP BaK122 as

follows. First, the flat feature around Γ point becomes clearly visible below T_c. Assuming the (π,π) folding, this can be attributed to the coherence of the electrons around X point being significantly enhanced by the onset of the superconductivity, as observed in the development of the EDC peaks in Fig. 1 (J and K). Second, the shift of E_{flat} (~6 meV) was observed just below T_c. This might be caused by the energy shift in the flat electron band under the condition of $\Delta_e/E_{bot} \approx 1$.

x-T phase diagram

Finally, we show that the indication of the antiferroic electronic instability is commonly observed from $x = 0.18$ to 0.6 in the BaK122 system. The x dependence of the E-k images around Γ point in the SC state is shown in Fig. 4A. The magnitudes of Δ_h and E_{flat} gradually decrease with increasing x. The characteristic x dependence was highlighted in the EDCs at the k_F of the inner hole band where the flat

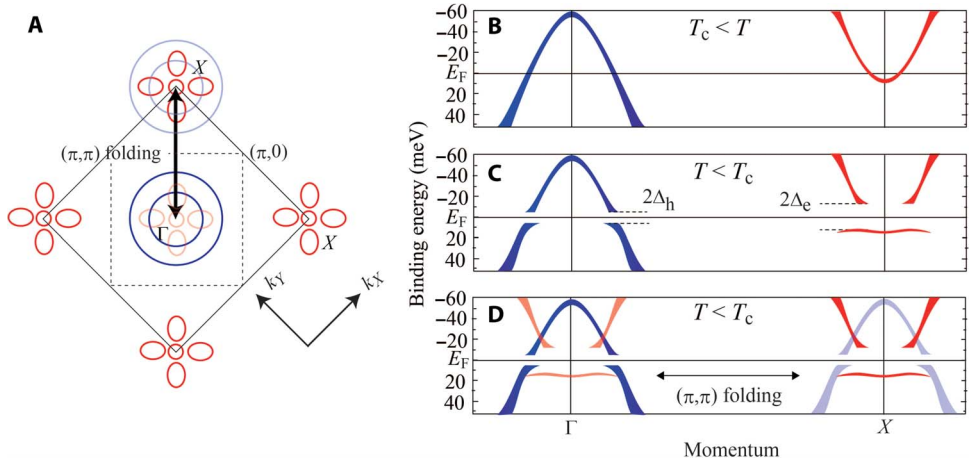

Fig. 3. Schematic of the (π,π) folding. (**A**) Schematic of the (π,π) folding in the BZ for $x = 0.41$. Folded FSs are indicated in light colors. k_X and k_Y represent the momentum axes with the tetragonal settings. (**B**) Simplified schematic of the hole and electron bands above T_c for $x = 0.41$. (**C**) The same as (B) but far below T_c. Δ_e and Δ_h represent the SC gaps of the electron and hole bands, respectively. (**D**) The same as (C) but in the presence of the (π,π) folding.

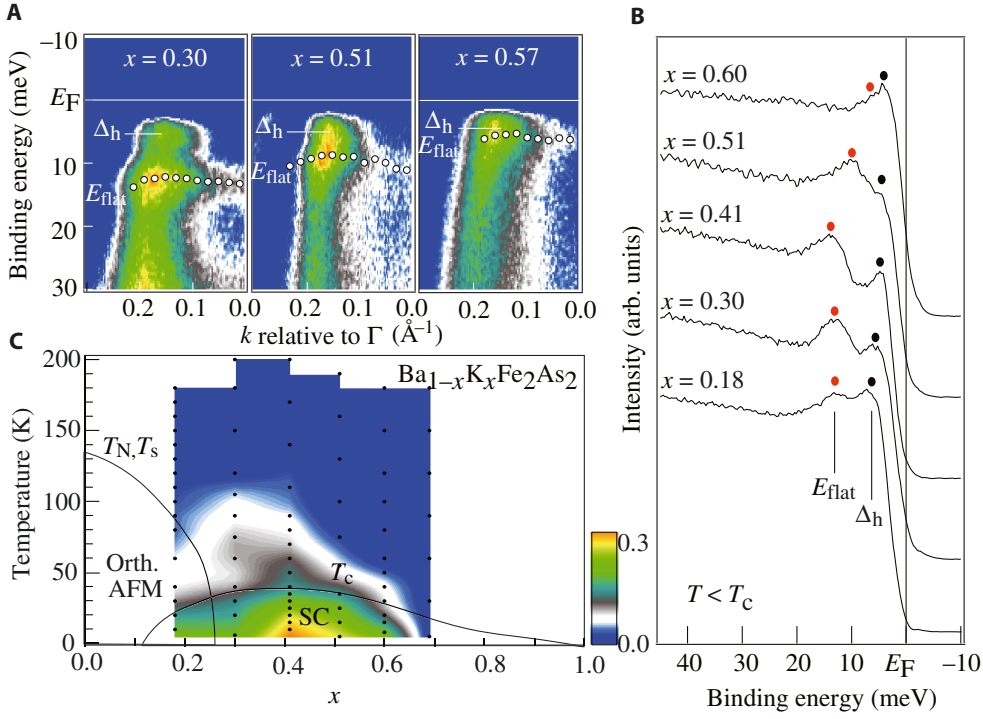

Fig. 4. *x* and *T* dependences of the flat intensity at Γ point. (**A**) E-k images around Γ point in the SC state for $x = 0.30$, 0.51, and 0.57 obtained by laser-ARPES ($h\nu$ = 6.994 eV). White circles represent the peak positions of the EDCs corresponding to the flat feature around Γ point. White horizontal lines show the location of the SC peak. (**B**) x dependence of the EDCs at the k_F of the inner hole band. Red and black markers represent the energy levels of the flat feature and SC gap, respectively. (**C**) Contour plot of the spectral weight derived from the flat feature around Γ point in the x-T phase diagram of the BaK122 system. The spectral weight was integrated between −5 and +5 meV around E_{flat} in the EDC at k_F of the inner hole band (section S5). The measurement points are indicated by black dots.

feature is clearly observed. As represented by the red circles in Fig. 4B, the flat feature shows continuous decrease in both energy and intensity with increasing x and almost disappears at $x \geq 0.6$. These behaviors support the scenario that the condition of $\Delta_e \approx E_{bot}$ is necessary for clearly detecting the replica of the electron band. With increasing x, Δ_e will decrease toward overdoped (OD) regime. At the same time, the electron band bottom at X point moves to the unoccupied state above $x \approx 0.5$ according to the rigid band picture reported by Neupane *et al.* (*33*). Therefore, the signature of the antiferroic electronic structure will be invisible above this threshold x, even if the electronic state still has a potential to exhibit the antiferroic instability.

In Fig. 4C, we present a x-T phase diagram showing the area where the signature of the replica electronic structure appears. The contour plot was obtained from the spectral weight at E_{flat} integrated with the energy window of ±5 meV in the EDCs divided by the Fermi-Dirac function at the k_F of the inner hole band (section S6). We note that the contour plot represents the inherent antiferroic electronic instability appearing through the replica structure being enhanced because of the condition of $\Delta_e \approx E_{bot}$ at X point. Figure 4C shows that the indication of the antiferroic replica structure clearly appears in the SC state, and its remnant is further observed above T_c (section S7).

DISCUSSION

The present results suggest that the influence of the antiferroic electronic instability appears in a wide area of the nonmagnetic phase in the BaK122 system, which should be distinguished from the signatures of the long-range AFM order exhibiting a strong competition with superconductivity (*31*, *40*–*42*). Alternatively, this instability may be related to the AFM fluctuations detected from underdoped to OD regime by the NMR measurements (*21*). The evolution of the AFM fluctuations (*21*) and transport property (*43*) of BaK122 show an anomaly around 100 K from OP to OD regime, which may be associated with the observed antiferroic instability (Fig. 4C). On the other hand, the elastic shear modulus indicating the nematic fluctuations [$\boldsymbol{q} \approx (0,0)$] was also observed in a wide range of x for BaK122 (*22*, *44*), which supports the presence of the nematic spin fluctuations (*12*). From the viewpoint of the orbital degrees of freedom, multiple orbital orders/fluctuations [$\boldsymbol{q} \approx (\pi,\pi)$ and $(0,0)$] can simultaneously develop with spin fluctuations, according to the theoretical studies based on the self-consistent vertex correction method (*17*). The antiferroic electronic instability observed in the present work suggests the presence of an as-yet-unknown electronic order, such as antiferroic orbital order, or some form of the nematic spin and/or orbital fluctuations, whose origin and relation to the high-T_c superconductivity should be further elucidated.

MATERIALS AND METHODS

Laser-ARPES measurements were performed on the spectrometer built using a VG-Scienta R4000WAL electron analyzer and a 6.994-eV vacuum ultraviolet laser as a photon source (*37*, *38*). Using the λ/2 (half-wave) plate, we could rotate the light polarization vector and obtain *s*- or *p*-polarized light. The energy resolution was set to 3 meV to obtain high count rate. ARPES measurements at the BZ corner were performed on the spectrometer built using a VG-Scienta R4000WAL electron analyzer, a motor-controlled six-axis manipulator, and a helium discharge lamp of $h\nu$ = 21.2 eV at the University of Tokyo. The energy resolution was set to 4 meV. The spectra were reproducible over measurement cycles (5 K ≤ T ≤ 200 K) of 24 hours. The E_F of samples was referenced to that of a gold film evaporated onto the sample substrate. All measurements were carried out on surfaces cleaved at 200 K in ultrahigh vacuum better than 5×10^{-11} torr. Single crystals of BaK122 ($0.18 \leq x \leq 0.69$) were grown by the self-flux method as described in detail by Ohgushi and Kiuchi (*43*) and Kihou *et al.* (*45*). The samples were mounted on the copper plate with a silver paste without applying pressure.

SUPPLEMENTARY MATERIALS

Supplementary material for this article is available at http://advances.sciencemag.org/cgi/content/full/3/8/e1700466/DC1

section S1. Band dispersions near X point
section S2. T dependence of the EDCs around X point divided by the Fermi-Dirac function
section S3. Intensity distribution of the flat feature around Γ point
section S4. Origin of the flat feature at Γ point
section S5. Band dispersion at X point for x = 0.51
section S6. x and T dependences of the EDCs at k_F of the inner hole band around Γ point
section S7. Contributions of the antiferroic instability in the ARPES data
fig. S1. Band structure across Γ-X line.
fig. S2. T dependence of the electron band at X point.
fig. S3. Intensity distribution around Γ point.
fig. S4. T dependence of the flat feature.
fig. S5. Band dispersions at Γ and X points for x = 0.51.
fig. S6. x and T dependences of the flat feature.
fig. S7. Normalized intensity of the flat feature.
fig. S8. Spectral intensity ratio between Γ and X points.

REFERENCES AND NOTES

1. Y. Kamihara, T. Watanabe, M. Hirano, H. Hosono, Iron-based layered superconductor $La[O_{1-x}F_x]FeAs$ (x = 0.05–0.12) with T_c = 26 K. *J. Am. Chem. Soc.* **130**, 3296–3297 (2008).
2. M. Rotter, M. Pangerl, M. Tegel, D. Johrendt, Superconductivity and crystal structures of $(Ba_{1-x}K_x)Fe_2As_2$ (x = 0–1). *Angew. Chem. Int. Ed.* **47**, 7949–7952 (2008).
3. Q. Huang, Y. Qiu, W. Bao, M. A. Green, J. W. Lynn, Y. C. Gasparovic, T. Wu, G. Wu, X. H. Chen, Neutron-diffraction measurements of magnetic order and a structural transition in the parent $BaFe_2As_2$ compound of FeAs-based high-temperature superconductors. *Phys. Rev. Lett.* **101**, 257003 (2008).
4. C. de la Cruz, Q. Huang, J. W. Lynn, J. Li, W. Ratcliff II, J. L. Zarestky, H. A. Mook, G. F. Chen, J. L. Luo, N. L. Wang, P. Dai, Magnetic order close to superconductivity in the iron-based layered $LaO_{1-x}F_xFeAs$ systems. *Nature* **453**, 899–902 (2008).
5. T. Shimojima, K. Ishizaka, Y. Ishida, N. Katayama, K. Ohgushi, T. Kiss, M. Okawa, T. Togashi, X.-Y. Wang, C.-T. Chen, S. Watanabe, R. Kadota, T. Oguchi, A. Chainani, S. Shin, Orbital-dependent modifications of electronic structure across the magnetostructural transition in $BaFe_2As_2$. *Phys. Rev. Lett.* **104**, 057002 (2010).
6. M. Yi, D. Lu, J.-H. Chu, J. G. Analytis, A. P. Sorini, A. F. Kemper, B. Moritz, S.-K. Mo, R. G. Moore, M. Hashimoto, W.-S. Lee, Z. Hussain, T. P. Devereaux, I. R. Fisher, Z.-X. Shen, Symmetry-breaking orbital anisotropy observed for detwinned $Ba(Fe_{1-x}Co_x)_2As_2$ above the spin density wave transition. *Proc. Natl. Acad. Sci. U.S.A.* **108**, 6878–6883 (2011).
7. K. Nakayama, Y. Miyata, G. N. Phan, T. Sato, Y. Tanabe, T. Urata, K. Tanigaki, T. Takahashi, Reconstruction of band structure induced by electronic nematicity in an FeSe superconductor. *Phys. Rev. Lett.* **113**, 237001 (2014).
8. F. Krüger, S. Kumar, J. Zaanen, J. van den Brink, Spin-orbital frustrations and anomalous metallic state in iron-pnictide superconductors. *Phys. Rev. B* **79**, 054504 (2009).
9. W. Lv, J. Wu, P. Phillips, Orbital ordering induces structural phase transition and the resistivity anomaly in iron pnictides. *Phys. Rev. B* **80**, 224506 (2009).
10. C.-C. Lee, W.-G. Yin, W. Ku, Ferro-orbital order and strong magnetic anisotropy in the parent compounds of iron-pnictide superconductors. *Phys. Rev. Lett.* **103**, 267001 (2009).
11. E. Fradkin, S. A. Kivelson, M. J. Lawler, J. P. Eisenstein, A. P. Mackenzie, Nematic Fermi fluids in condensed matter physics. *Annu. Rev. Condens. Matter Phys.* **1**, 153–178 (2010).
12. R. M. Fernandes, A. V. Chubukov, J. Schmalian, What drives nematic order in iron-based superconductors? *Nat. Phys.* **10**, 97–104 (2014).
13. C. Fang, H. Yao, W.-F. Tsai, J. Hu, S. A. Kivelson, Theory of electron nematic order in LaFeAsO. *Phys. Rev. B* **77**, 224509 (2008).
14. R. M. Fernandes, L. H. VanBebber, S. Bhattacharya, P. Chandra, V. Keppens, D. Mandrus, M. A. McGuire, B. C. Sales, A. S. Sefat, J. Schmalian, Effects of nematic fluctuations on the elastic properties of iron arsenide superconductors. *Phys. Rev. Lett.* **105**, 157003 (2010).
15. R. M. Fernandes, A. E. Böhmer, C. Meingast, J. Schmalian, Scaling between magnetic and lattice fluctuations in iron pnictide superconductors. *Phys. Rev. Lett.* **111**, 137001 (2013).

16. H. Kontani, T. Saito, S. Onari, Origin of orthorhombic transition, magnetic transition, and shear-modulus softening in iron pnictide superconductors: Analysis based on the orbital fluctuations theory. *Phys. Rev. B* **84**, 024528 (2011).
17. S. Onari, H. Kontani, Self-consistent vertex correction analysis for iron-based superconductors: Mechanism of coulomb interaction-driven orbital fluctuations. *Phys. Rev. Lett.* **109**, 137001 (2012).
18. S.-H. Baek, D. V. Efremov, J. M. Ok, J. S. Kim, J. van den Brink, B. Büchner, Orbital-driven nematicity in FeSe. *Nat. Mater.* **14**, 210–214 (2015).
19. J.-H. Chu, J. G. Analytis, K. De Greve, P. L. McMahon, Z. Islam, Y. Yamamoto, I. R. Fisher, In-plane resistivity anisotropy in an underdoped iron arsenide superconductor. *Science* **329**, 824–826 (2010).
20. S. Kasahara, H. J. Shi, K. Hashimoto, S. Tonegawa, Y. Mizukami, T. Shibauchi, K. Sugimoto, T. Fukuda, T. Terashima, A. H. Nevidomskyy, Y. Matsuda, Electronic nematicity above the structural and superconducting transition in $BaFe_2(As_{1-x}P_x)_2$. *Nature* **486**, 382–385 (2012).
21. M. Hirano, Y. Yamada, T. Saito, R. Nagashima, T. Konishi, T. Toriyama, Y. Ohta, H. Fukazawa, Y. Kohori, Y. Furukawa, K. Kihou, C.-H. Lee, A. Iyo, H. Eisaki, Potential antiferromagnetic fluctuations in hole-doped iron-pnictide superconductor $Ba_{1-x}K_xFe_2As_2$ studied by ^{75}As nuclear magnetic resonance measurement. *J. Phys. Soc. Jpn.* **81**, 054704 (2012).
22. A. E. Böhmer, P. Burger, F. Hardy, T. Wolf, P. Schweiss, R. Fromknecht, M. Reinecker, W. Schranz, C. Meingast, Nematic susceptibility of hole-doped and electron-doped $BaFe_2As_2$ iron-based superconductors from shear modulus measurements. *Phys. Rev. Lett.* **112**, 047001 (2014).
23. Y. K. Kim, W. S. Jung, G. R. Han, K.-Y. Choi, C.-C. Chen, T. P. Devereaux, A. Chainani, J. Miyawaki, Y. Takata, Y. Tanaka, M. Oura, S. Shin, A. P. Singh, H. G. Lee, J.-Y. Kim, C. Kim, Existence of orbital order and its fluctuation in superconducting $Ba(Fe_{1-x}Co_x)_2As_2$ single crystals revealed by x-ray absorption spectroscopy. *Phys. Rev. Lett.* **111**, 217001 (2013).
24. H. Ding, P. Richard, K. Nakayama, K. Sugawara, T. Arakane, Y. Sekiba, A. Takayama, S. Souma, T. Sato, T. Takahashi, Z. Wang, X. Dai, Z. Fang, G. F. Chen, J. L. Luo, N. L. Wang, Observation of Fermi-surface–dependent nodeless superconducting gaps in $Ba_{0.6}K_{0.4}Fe_2As_2$. *Europhys. Lett.* **83**, 47001 (2008).
25. L. Zhao, H.-Y. Liu, W.-T. Zhang, J.-Q. Meng, X.-W. Jia, G.-D. Liu, X.-L. Dong, G.-F. Chen, J.-L. Luo, N.-L. Wang, W. Lu, G.-L. Wang, Y. Zhou, Y. Zhu, X.-Y. Wang, Z.-Y. Xu, C.-T. Chen, X.-J. Zhou, Multiple nodeless superconducting gaps in $(Ba_{0.6}K_{0.4})Fe_2As_2$ superconductor from angle-resolved photoemission spectroscopy. *Chin. Phys. Lett.* **25**, 4402–4405 (2008).
26. D. V. Evtushinsky, D. S. Inosov, V. B. Zabolotnyy, A. Koitzsch, M. Knupfer, B. Büchner, M. S. Viazovska, G. L. Sun, V. Hinkov, A. V. Boris, C. T. Lin, B. Keimer, A. Varykhalov, A. A. Kordyuk, S. V. Borisenko, Momentum dependence of the superconducting gap in $Ba_{1-x}K_xFe_2As_2$. *Phys. Rev. B* **79**, 054517 (2009).
27. Y. Zhang, L. X. Yang, F. Chen, B. Zhou, X. F. Wang, X. H. Chen, M. Arita, K. Shimada, H. Namatame, M. Taniguchi, J. P. Hu, B. P. Xie, D. L. Feng, Out-of-plane momentum and symmetry-dependent energy gap of the pnictide $Ba_{0.6}K_{0.4}Fe_2As_2$ superconductor revealed by angle-resolved photoemission spectroscopy. *Phys. Rev. Lett.* **105**, 117003 (2010).
28. T. Shimojima, F. Sakaguchi, K. Ishizaka, Y. Ishida, T. Kiss, M. Okawa, T. Togashi, C.-T. Chen, S. Watanabe, M. Arita, K. Shimada, H. Namatame, M. Taniguchi, K. Ohgushi, S. Kasahara, T. Terashima, T. Shibauchi, Y. Matsuda, A. Chainani, S. Shin, Orbital-independent superconducting gaps in iron pnictides. *Science* **332**, 564–567 (2011).
29. D. V. Evtushinsky, T. K. Kim, A. A. Kordyuk, V. B. Zabolotnyy, B. Büchner, A. V. Boris, D. L. Sun, C. T. Lin, H. Q. Luo, Z. S. Wang, H. H. Wen, R. Follath, S. V. Borisenko, Fusion of bogoliubons in $Ba_{1-x}K_xFe_2As_2$ and similarity of energy scales in high temperature superconductors. arXiv:1106.4584 (2011).
30. W. Malaeb, T. Shimojima, Y. Ishida, K. Okazaki, Y. Ota, K. Ohgushi, K. Kihou, T. Saito, C. H. Lee, S. Ishida, M. Nakajima, S. Uchida, H. Fukazawa, Y. Kohori, A. Iyo, H. Eisaki, C.-T. Chen, S. Watanabe, H. Ikeda, S. Shin, Abrupt change in the energy gap of superconducting $Ba_{1-x}K_xFe_2As_2$ single crystals with hole doping. *Phys. Rev. B* **86**, 165117 (2012).
31. M. Yi, Y. Zhang, Z.-K. Liu, X. Ding, J.-H. Chu, A. F. Kemper, N. Plonka, B. Moritz, M. Hashimoto, S.-K. Mo, Z. Hussain, T. P. Devereaux, I. R. Fisher, H.-H. Wen, Z.-X. Shen, D. H. Lu, Dynamic competition between spin-density wave order and superconductivity in underdoped $Ba_{1-x}K_xFe_2As_2$. *Nat. Commun.* **5**, 3711 (2014).
32. P. Zhang, P. Richard, T. Qian, X. Shi, J. Ma, L.-K. Zeng, X.-P. Wang, E. Rienks, C.-L. Zhang, P. Dai, Y.-Z. You, Z.-Y. Weng, X.-X. Wu, J. P. Hu, H. Ding, Observation of momentum-confined in-gap impurity state in $Ba_{0.6}K_{0.4}Fe_2As_2$: Evidence for antiphase $s_\pm$ pairing. *Phys. Rev. X* **4**, 031001 (2014).
33. M. Neupane, P. Richard, Y.-M. Xu, K. Nakayama, T. Sato, T. Takahashi, A. V. Federov, G. Xu, X. Dai, Z. Fang, Z. Wang, G.-F. Chen, N.-L. Wang, H.-H. Wen, H. Ding, Electron-hole asymmetry in the superconductivity of doped $BaFe_2As_2$ seen via the rigid chemical-potential shift in photoemission. *Phys. Rev. B* **83**, 094522 (2011).
34. Y. Lubashevsky, E. Lahoud, K. Chashka, D. Podolsky, A. Kanigel, Shallow pockets and very strong coupling superconductivity in $FeSe_xTe_{1-x}$. *Nat. Phys.* **8**, 309–312 (2012).
35. K. Okazaki, Y. Ito, Y. Ota, Y. Kotani, T. Shimojima, T. Kiss, S. Watanabe, C.-T. Chen, S. Niitaka, T. Hanaguri, H. Takagi, A. Chainani, S. Shin, Superconductivity in an electron band just above the Fermi level: Possible route to BCS-BEC superconductivity. *Sci. Rep.* **4**, 4109 (2014).
36. S. Kasahara, T. Watashige, T. Hanaguri, Y. Kohsaka, T. Yamashita, Y. Shimoyama, Y. Mizukami, R. Endo, H. Ikeda, K. Aoyama, T. Terashima, S. Uji, T. Wolf, H. von Löhneysen, T. Shibauchi, Y. Matsuda, Field-induced superconducting phase of FeSe in the BCS-BEC cross-over. *Proc. Natl. Acad. Sci. U.S.A.* **111**, 16309–16313 (2014).
37. T. Kiss, T. Shimojima, K. Ishizaka, A. Chainani, T. Togashi, T. Kanai, X.-Y. Wang, C.-T. Chen, S. Watanabe, S. Shin, A versatile system for ultrahigh resolution, low temperature, and polarization dependent laser-angle-resolved photoemission spectroscopy. *Rev. Sci. Instr.* **79**, 023106 (2008).
38. T. Shimojima, K. Okazaki, S. Shin, Low-temperature and high-energy-resolution laser photoemission spectroscopy. *J. Phys. Soc. Jpn.* **84**, 072001 (2015).
39. K. Suzuki, H. Usui, K. Kuroki, Possible three-dimensional nodes in the s± superconducting gap of $BaFe_2(As_{1-x}P_x)_2$. *J. Phys. Soc. Jpn.* **80**, 013710 (2011).
40. C. Liu, T. Kondo, R. M. Fernandes, A. D. Palczewski, E. D. Mun, N. Ni, A. N. Thaler, A. Bostwick, E. Rotenberg, J. Schmalian, S. L. Bud'ko, P. C. Canfield, A. Kaminski, Evidence for a Lifshitz transition in electron-doped iron arsenic superconductors at the onset of superconductivity. *Nat. Phys.* **6**, 419–423 (2010).
41. D. K. Pratt, W. Tian, A. Kreyssig, J. L. Zarestky, S. Nandi, N. Ni, S. L. Bud'ko, P. C. Canfield, A. I. Goldman, R. J. McQueeney, Coexistence of competing antiferromagnetic and superconducting phases in the underdoped $Ba(Fe_{0.953}Co_{0.047})_2As_2$ compound using x-ray and neutron scattering techniques. *Phys. Rev. Lett.* **103**, 087001 (2009).
42. A. D. Christianson, M. D. Lumsden, S. E. Nagler, G. J. MacDougall, M. A. McGuire, A. S. Sefat, R. Jin, B. C. Sales, D. Mandrus, Static and dynamic magnetism in underdoped superconductor $BaFe_{1.92}Co_{0.08}As_2$. *Phys. Rev. Lett.* **103**, 087002 (2009).
43. K. Ohgushi, Y. Kiuchi, Doping dependence of Hall coefficient and evolution of coherent electronic state in the normal state of the Fe-based superconductor $Ba_{1-x}K_xFe_2As_2$. *Phys. Rev. B* **85**, 064522 (2012).
44. H.-H. Kuo, J.-H. Chu, J. C. Palmstrom, S. A. Kivelson, I. R. Fisher, Ubiquitous signatures of nematic quantum criticality in optimally doped Fe-based superconductors. *Science* **352**, 958–962 (2016).
45. K. Kihou, T. Saito, S. Ishida, M. Nakajima, Y. Tomioka, H. Fukazawa, Y. Kohori, T. Ito, S.-i. Uchida, A. Iyo, C.-H. Lee, H. Eisaki, Single crystal growth and characterization of the iron-based superconductor KFe_2As_2 synthesized by KAs flux method. *J. Phys. Soc. Jpn.* **79**, 124713 (2010).

Acknowledgments: We thank T. Shibauchi and H. Kontani for valuable discussions. We also acknowledge K. Ono and H. Kumigashira for the experimental support at the Photon Factory. **Funding:** This work was supported by the Photon and Quantum Basic Research Coordinated Development Program of the MEXT (Ministry of Education, Culture, Sports, Science and Technology), the Photon Frontier Network Program of the MEXT, and Research Hub for Advanced Nano Characterization, the University of Tokyo (supported by MEXT), Japan and by a Grant-in-Aid for Scientific Research from the Japan Society for the Promotion of Science, Japan (KAKENHI grant nos. 25220707 and 15H03687). **Author contributions:** T.S., W.M., K.I., and S.S. designed the research. T.S., W.M., and A.N. performed the ARPES measurements and analyzed the data. K.K., C.-H.L., A.I., H.E., S.I., M.N., S.U., and K.O. synthesized the single crystals. T.S., T.K., K.I., and S.S. set up the ARPES apparatus. T.S. wrote the paper with inputs from W.M., A.N., T.K., H.E., K.O., K.I., and S.S. **Competing interests:** The authors declare that they have no competing interests. **Data and materials availability:** All data needed to evaluate the conclusions in the paper are present in the paper and/or the Supplementary Materials. Additional data related to this paper may be requested from the authors.

Submitted 12 February 2017
Accepted 1 August 2017
Published 25 August 2017
10.1126/sciadv.1700466

Citation: T. Shimojima, W. Malaeb, A. Nakamura, T. Kondo, K. Kihou, C.-H. Lee, A. Iyo, H. Eisaki, S. Ishida, M. Nakajima, S.-i. Uchida, K. Ohgushi, K. Ishizaka, S. Shin, Antiferroic electronic structure in the nonmagnetic superconducting state of the iron-based superconductors. *Sci. Adv.* **3**, e1700466 (2017).